JOURNAL OF CATALYSIS 35, 100–114 (1974)

Photoelectric Work Functions of Silver Catalysts and Silver Catalysts Modified by Addition of Alkaline Earth Compounds

H. T. SPATH, K. MAYER AND K. TORKAR

Institut für Physikalische und Theoretische Chemie, Technische Hochschule, Graz, Austria

Received July 25, 1973; revised January 4, 1974

The photoelectric work function Ψ of silver catalysts modified by addition of 2–20 mole% of Ba and Sr peroxide, formate and carbonate is markedly reduced, the steepest decrease in Ψ being at small additive concentration. At 6–8 mole% addition Ψ approaches a stationary value. Changes in Ψ are more pronounced with peroxides and type I (alcohol) preparation ($\Delta\Psi \simeq -0.6$ eV) as compared to addition of the inert carbonate ($\Delta\Psi \simeq -0.3$ eV). An intermediate situation is met with formates and type II (acetone) preparation. On conditioning the catalyst components in a stream of ethylene/air at 300°C, the peroxides and formates transform into their respective carbonate. The carbonate covers the underlying silver with a thin film which, by incorporation of silver atoms acting as donors, is endowed with semiconducting properties. The interpretation of the work function vs mole percent additive characteristics is based upon the model of a metal/semiconductor film contact. Calculations of the electrostatic potential across the film and at its catalytically active outer surface (in the absence or presence of an acceptor gas) satisfactorily reflect the experimental findings.

INTRODUCTION

In two previous papers (*1*, *2*) the mechanism of the action of alkaline earth additives to silver catalysts used in the direct oxidation of ethylene to ethylene oxide and to $CO_2 + H_2O$ has been described. The discussion was essentially based upon changes in the surface properties (surface area, topology) on addition of 2–20 mole% of the peroxides, formates, oxalates and carbonates with respect to a properly defined pure standard silver catalyst, although from the catalytic behavior (activity, selectivity) and scanning electron micrographs possible changes in the electronic properties of the actual catalyst surface were suggested. From scanning electron micrographs it was concluded that the actual catalyst matrix in compound catalysts consists of a thin semiconducting carbonate film (probably of *n*-type characteristics) in intimate electrical contact with the underlying metallic silver. It was in this way that the increase in activity per unit surface area of compound silver catalysts was tentatively explained.

The aim of the present study was to obtain some insight into the electronic structure of silver catalysts modified by addition of the above mentioned additives (2–20 mole%) from photoelectric work function measurements. Changes in work function have been well established with silver catalysts containing small amounts (<0.1%) of Cl, S, Te and other electronegative or electropositive elements with respect to silver (*3*, *4*) and qualitative relationships to corresponding changes in activity and selectivity have been put forward. However, so far as we know, no attempt has been made in this direction with silver catalysts containing additives of the above-mentioned type and present to far larger amounts although these catalysts are of considerable commercial importance, and their properties have been repeatedly discussed in the current and patent literature (*5–12*).

A knowledge of the position of the Fermi level as revealed from work function data is important for interpreting the chemisorption characteristics of the reacting gases (especially of oxygen) and essentially determines the oxidation capacity of the catalyst surface to oxidize ethylene to either ethylene oxide or to the undesired side products $CO_2 + H_2O$.

The work function Ψ of the catalysts under vacuum conditions has been determined employing the photoelectric method. The work function, defined as the minimum energy required to remove an electron from the inside of a solid to a point just outside its surface, is the sum of the chemical potential μ (including contributions from image forces) and the surface potential energy $-e\chi$. For semiconductors, in addition, the diffusion potential energy $-e\phi$ originating from a space charge region must be accounted for. The surface potential not only depends on the crystal faces and surface structure but is strongly altered by any contamination of the surface, e.g., by chemisorbed molecules or atoms. Determination of an absolute value of Ψ thus requires clean and homogeneous surfaces. This can be achieved with ultrahigh vacuum and with repeated heating to high temperatures [above 500°C in case of silver to remove residual oxygen (*13*)]. However, in this study we were interested mainly to determine *changes in work function* of the *actual compound catalysts* (containing increasing amounts of an additive) *relative to* a *properly defined silver catalyst* under constant and standardized conditions widely approaching those of *actual catalytic reaction*. For this purpose less rigorous experimental pretentions were envisaged, i.e., the catalyst samples were generally not heated above 300–350°C in order to preserve the catalyst matrix existing under reaction conditions (200–300°C) and therefore a vacuum of not better than 10^{-6} Torr could be maintained over the samples. On the other hand, in actual catalysts there is never a homogeneous surface. It has been shown, e.g., by Kummer (*14*), that defined crystal faces of silver quickly become randomly orientated during reaction. This surface heterogeneity is still more pronounced with compound catalysts (*1*). Thus the work function data reported here are to be considered as experimental quantities representing an average value over the "patchy" catalyst surface.

Experimental Methods

Materials

The materials used were the same as described previously (*1*, *2*). Again, two types of preparation were employed. The homogenized starting materials (AgO + additive) resulting from either alcohol (type I) or acetone (type II) suspensions were conditioned in a stream of ethylene/air (3–4 vol% ethylene) at 300°C for about 15 hr. The conditioned catalyst powders were compressed to thin pellets (0.5–1 mm thick) onto the nickel sample carrier of the phototube (photocathode) at a pressure of 15–20 kg/cm^2. As pointed out previously (*1*, *2*) the peroxides and formates quantitatively transform into their respective carbonates during the conditioning process, whereas this is only partially true for the oxalates.

Method

The photoelectric work function is calculated from recordings of the photoelectric yield Y_ν vs frequency ν functions in a frequency range $\Delta\nu$ around the threshold ν_0. In this study, instead of yields emission currents I_ν for *constant incident photon energy* E_ν have been recorded. I_ν is proportional to Y_ν if one makes the justified assumption that the optical absorption of the samples is constant over the narrow wave length range involved (230–300 nm). The true work function Ψ_0, i.e., that referring to 0°K, from I_ν vs ν data recorded at any constant cathode temperature $T > 0$ is calculated graphically by a method due to Fowler (*15*). According to Fowler the quantity $\ln(I_\nu/T^2)$ is related to a universal function $f(u)$ by the equation

$$\ln(I_\nu/T^2) = B + f(u), \qquad (1)$$

where $u = h(\nu - \nu_0)/kT$ (h and k are Planck's and Boltzmann's constants, respectively). To evaluate $\Psi_0 = h\nu_0$, a plot of

$\ln(I_\nu/T^2)$ vs $h\nu/kT$ is brought into coincidence with the theoretical Fowler function $f(u)$ by shifting the latter horizontally and vertically. The horizontal shift equals $h\nu_0/kT$, whereas from the vertical shift the emission constant B is obtained. The procedure is illustrated in Fig. 1 for a silver catalyst originally containing 1.3 mole% BaO_2. $\emptyset_A$ and $\emptyset_B$ indicate the zeros of coordinates of the shifted theoretical Fowler function. In this way the true work function $\Psi_0 = h\nu_0$ (in eV) is immediately obtained. The accuracy of the method is within ± 0.02 eV.

An alternative to this method is to construct a plot of $I_\nu^{1/2}$ vs $h\nu$ corresponding to the simplified Fowler equation

$$I_\nu \propto \frac{(h\nu - \Psi_0)^2}{(\theta - h\nu)^{1/2}} \qquad (2)$$

(θ is the distance from the bottom of the valence band to the zero of energy). Equation (2) is an approximation valid at $T \to 0$ and $h\nu \gg h\nu_0$, the denominator being almost constant. Figure 2 illustrates the validity of Eq. (2) for a silver catalyst originally containing 2 mole% Sr-formate at two cathode temperatures. The accuracy of the method again is within ± 0.02 eV.

The two procedures, in principle, are applicable only for metals. However, it is evident from Figs. 1 and 2 that both methods equally well apply to compound catalysts. This point is essential in view of the interpretation of the results.

The following data, obtained at two temperatures for a silver catalyst originally containing 2 mole% Sr-formate, summarize the reliability of the two methods under discussion:

	Ψ_0 (250°C)	Ψ_0 (350°C)
Eq. (1)	4.05 eV	4.07 eV
Eq. (2)	4.07 eV	4.09 eV

Apparatus and Procedure

A block diagram of the experimental equipment employed is shown in Fig. 3. Light from a high pressure mercury lamp (Osram HBO 500 W/2) with sufficient intensity over the wave length range of interest (230–300 nm) passes through a ¼ m Jarrell Ash grating monochromator

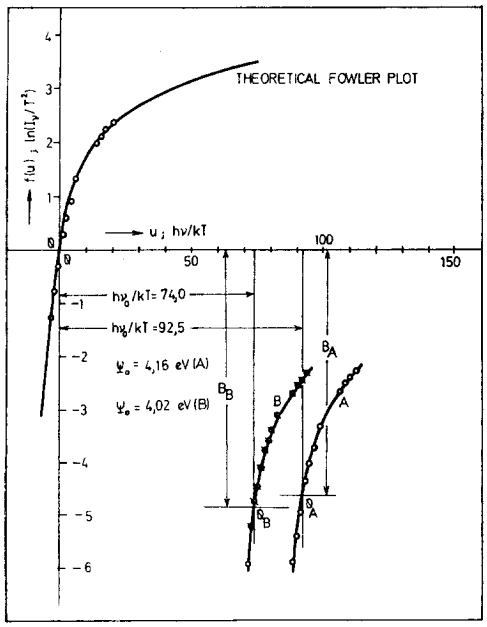

FIG. 1. Determination of Ψ_0 according to Eq. (1) for a catalyst originally containing 1.3 mole% BaO_2 (type I). Cathode temperature: 250°C (A) and 350°C (B).

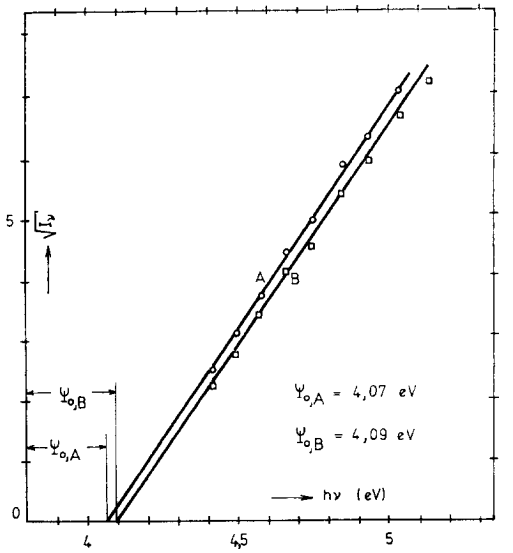

FIG. 2. Determination of Ψ_0 according to Eq. (2) for a catalyst originally containing 2 mole% Sr-formate (type II). Cathode temperature: 250°C (A) and 350°C (B).

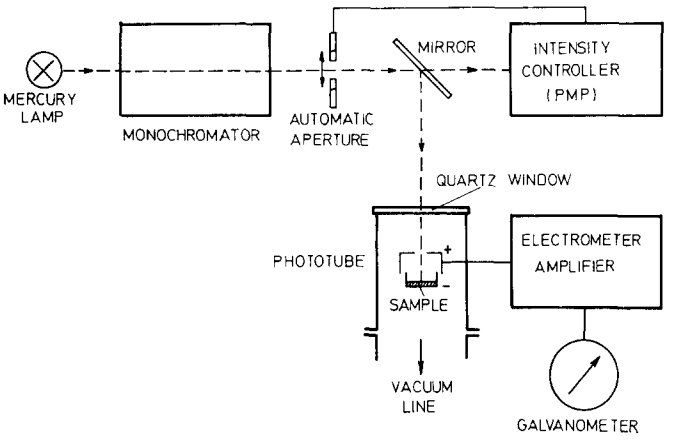

FIG. 3. Block diagram of the experimental equipment.

(with resolution of 5 nm at the circular aperture of 1–2.5 mm used) and is focused on the photocathode by means of a semipermeable mirror. A constant portion of the photon energy passes the mirror and strikes the tube of a photomultiplier (type 150 UVP, Valvo) calibrated against a thermopile. The output of the multiplier, after amplification, is compared to a given voltage, and corresponding to the difference in the two voltages and its sign the extent of opening of an aperture is controlled automatically until the selected constant photon energy is obtained.

The phototube used is shown in Fig. 4. After passing through the plane parallel quartz window 1, sealed to the glass cylinder 2, and the bored collector electrode 3, the light strikes the catalyst pellet 4 compressed onto the nickel carrier electrode 5 (photocathode). Heating of the photocathode is performed by a Thermocoax winding 6. The temperature is controlled by a Varian Aerograph Model 328 temperature controller (via a platinum resistance thermometer 7) to an accuracy of $\pm 1°C$ and measured by a thermocouple/thermocompensator unit 8. The collector electrode is held by two quartz rods 9 which at the same time ensure the necessary insulation ($>10^{16}$ ohms) required for accurate measurements of photocurrents in the order of 10^{-12} to 10^{-15} A. A metal cylinder 10 protects the phototube from external electromagnetic fields. The base plane of the phototube is water cooled.

The emitted photoelectrons are collected by the anode 3 held at a potential of +100 V across the resistance 11 of 2×10^9 ohms. The photocurrent is amplified by an electrometer tube 12 (RCA 4065) by a factor of about 10^6. Both the resistance and the electrometer tube are arranged *within* the phototube to minimize any possible dis-

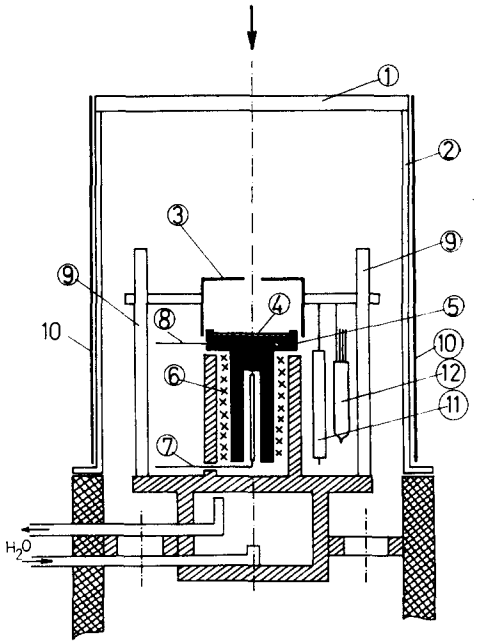

FIG. 4. Phototube.

turbances. A condenser (not shown in Fig. 4) of 1000 pF capacity parallel to the resistance 11 protects the circuit from disturbing ac fields arising from the heating wires 6. The amplified photocurrent recorded by a galvanometer (sensitivity 5×10^{-10} A), as pointed out above, is directly proportional to the photoelectric yield. The overall sensitivity of the device for photocurrent measurements is around 10^{-15} A. Minor modifications of the electrode arrangement enables conductivity and photoconductivity measurements to be made on the sample pellets. The phototube is connected to a high vacuum system consisting of a two stage rotary and a three stage oil diffusion pump (Leybold PD 251) providing a vacuum around 10^{-6} Torr after an outgassing period of 6–10 hr. The vacuum is measured by a Leybold IM III ionization gauge. A cathode/sample temperature of 250°C was selected, since this was the average temperature of the catalytic investigations (*1*, *2*). In order to detect a possible dependence of the work function on the cathode temperature for compound catalysts, the measurements were repeated at 350°C. With vacuum and temperature conditions set up, the photocurrent vs frequency functions were recorded at 5 nm intervals.

Results

Pure Silver Catalysts

The work function of pure silver catalysts strongly depends on the preparation and pretreatment of the samples. Literature data from 4.08 to 4.7 eV have been reported (*16–19*). The work function also differs with different crystal planes (*16*). Therefore, direct comparison of literature data with work functions reported here for polycrystalline material should be made with caution, the more so since the silver catalysts under discussion may contain traces of sulphur from the preparation of the AgO (this, however, has a favorable effect on selectivity). On the other hand, at 250°C and 10^{-6} Torr residual pressure it is not possible to remove oxygen quantitatively from the silver surface. This, in addition, may cause deviations from a "true" work function of "pure" silver. Nevertheless, reliable values for the work function of a standard "pure" silver catalyst were obtained by strictly standardizing preparation, pretreatment (conditioning) and measuring conditions.

With silver from AgO a constant emission current at a selected wave length (240 nm) is arrived at within 0.5–1 hr (desorption of oxygen). After that period well reproducible emission characteristics were observed. The results for various samples are summarized in Table 1. Samples 1–5 were taken from the same AgO preparation batch, samples 6 and 7 from two other batches. Silver for sample 9 was obtained from Ag_2CO_3. As seen from Table 1 the differences in Ψ_0 for type I and type II catalysts lie within experimental error and, as expected for a metal, Ψ does not depend on the cathode temperature.

TABLE 1

Work Function of Various Silver Samples (Type I and II) Obtained from Different Preparations at Two Cathode Temperatures

Sample	Starting material	Type of preparation	Ψ_0 (250°C) (eV)	Ψ_0 (350°C) (eV)
1	AgO	Thermal decomposition	4.43	—
2	AgO	I	4.44	4.38
3	AgO	I	4.47	4.42
4	AgO	II	4.40	4.40
5	AgO	II	—	4.38
6	AgO	I	4.12	—
7	AgO	II	4.03	4.02
9	Ag_2CO_3	I	4.35	4.43

However, a pronounced difference is obtained within different batches of AgO. Ψ_0 for samples 1–5 agree well with the most reliable values reported (4.40–4.50 eV) indicating that these specimens were almost "pure" silver. This, in addition, was proved by comparison with Ψ_0 for silver obtained from A.R. grade Ag_2CO_3 (sample 9). Samples 6 and 7, taken from obviously less pure AgO (possible contaminations by sulfur and alkali metals) have considerably lower work functions. Therefore, the compound catalysts discussed in the following section were all prepared from AgO taken from the first batch and the average of Ψ_0 from samples 2–5 was used as a comparative standard. It should be mentioned that Ψ_0 was not sensitive to minor variations of the vacuum from 2×10^{-5} to 10^{-6} Torr.

Compound Silver Catalysts

Appreciable photocurrents from compound silver catalysts were not observed below 150°C, especially at low additive concentration. Up to 250°C the emission currents steadily rise and slowly approach a stationary value. This, probably, is due to stronger oxygen chemisorption as compared to pure silver. On illumination, oxygen desorption at 250°C is enhanced by photoelectrons. Similar observations have been reported by Millikan (*20*) and Winch (*21*).

From the emission current vs frequency data the work function Ψ_0 could again be calculated from Fowler plots (Figs. 1 and 2). The results for different catalyst series containing varying amounts of Ba and Sr additives are compiled in Table 2. The characteristic features are illustrated in Figs. 5 and 6 and can be summarized as follows:

1. With increasing amounts of an additive not stable in a stream of ethylene/air at reaction conditions (220–300°C) but transforming into the respective carbonate (peroxides, formates) the work function markedly decreases (the steepest decrease being observed at small additive concentrations) and approaches a constant value around 6–8 mole% addition. Decrease in Ψ_0 is more

TABLE 2

WORK FUNCTION OF SILVER CATALYSTS CONTAINING VARYING AMOUNTS OF DIFFERENT ADDITIVES[a]

Additive	Mole%	Type of preparation	Ψ_0 (250°C)	Ψ_0 (350°C)
$BaCO_3$	0.7	(a), I	4.14 (300°C)	
	1.3	(a), I	4.17	
	2.6	(a), I	4.12	
	5.0	(a), I	4.10	
	6.6	(a) I	4.14	
	10.1	(a), I	4.10	
$BaCO_3$	1.3	(b), I	4.39	4.28
	2.6	(b), I	4.36	4.26
	5.2	(b), I	4.28	4.26
	8.0	(b), I	4.15	4.20
	10.1	(b), I	4.20	4.18
	17.5	(b), I	4.10	4.08
BaO_2	1.3	(b), I	4.16	4.02
	3.0	(b), I	3.87	3.70
	5.2	(b), I	3.82	3.75
	10.1	(b), I	3.78	3.80
	3.0	(b), II	4.10	4.13
	3.2	(b), II	4.05	4.13
	5.2	(b), II	3.98	3.95

[a] $\Psi_0 = 4.20$ eV for Ag used in the series $Ag/BaCO_3$, thermally decomposed, and $\Psi_{0,Ag} = 4.45$ eV for the other series. (a) Thermally decomposed; (b) conditioned in ethylene/air.

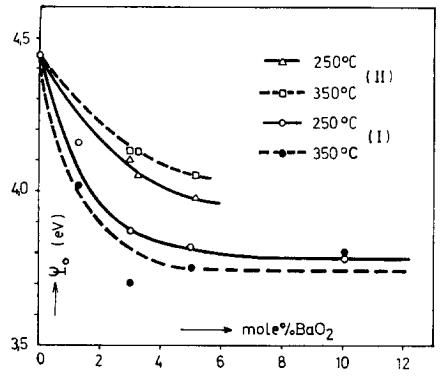

FIG. 5. Work function of type I and type II Ag/BaO_2 catalysts determined at 250 and 350°C.

pronounced with type I than with type II preparation.

2. Comparing Ba and Sr additives (Table 3) it is seen that the work function vs mole% additive characteristics do not depend on the cation. The decrease in work function must therefore be governed by some *common feature.*

3. With catalysts containing small amounts of an additive, Ψ_0 was found to depend somewhat on the cathode temperature (Fig. 6), whereby for type I catalysts $\Psi_{0,350°C} < \Psi_{0,250°C}$ and for type II catalysts $\Psi_{0,350°C} > \Psi_{0,250°C}$. For a catalyst originally containing 1.3 mole% BaO_2, Ψ_0 decreased from 4.16 eV at 250°C to 4.02 eV at 350°C. A stationary value at the new temperature was reached within about 5 hr. On cooling to 250°C Ψ_0 resettled at 4.12 eV. For catalysts containing larger additive concentrations changes in Ψ_0 with cathode temperature fall within the experimental errors.

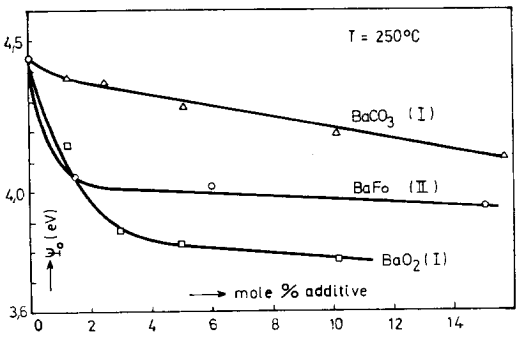

FIG. 6. Changes in work function for Ag/BaO_2 (type I), Ag/Ba-formate (type II) and $Ag/BaCO_3$ (type I) catalysts determined at 250°C.

TABLE 3
COMPARATIVE SURVEY OF WORK FUNCTIONS DETERMINED FOR CATALYSTS CONTAINING EQUAL AMOUNTS OF Sr AND Ba ADDITIVES (TYPE II PREPARATION)

Additive	Mole%	Ψ_0 (250°C) (eV)	Ψ_0 (350°C) (eV)
Ba			
peroxide	5.2	3.98	3.95
formate	2.0	4.05	4.18
formate	6.0	4.03	4.10
formate	8.0	4.18	4.20
formate	15.0	3.94	4.02
Sr			
peroxide	5.2	4.05	4.15
formate	2.0	4.05	4.07
formate	6.0	4.10	4.15
formate	8.0	4.18	4.18
formate	15.0	4.10	4.10

4. With *direct addition* of the *inert* $BaCO_3$ and *thermal decomposition* of the AgO component in N_2 at 400°C only a very small decrease in Ψ_0 was observed. Incidentally, in this case silver with $\Psi_0 = 4.2$ eV was used (cf. Table 2). On the other hand, *conditioning in ethylene/air* of the $AgO/BaCO_3$ mixture (type I) in the usual manner causes a noticeable decrease in Ψ_0, addition of 17.5 mole% $BaCO_3$ producing about the same decrease in Ψ_0 as does 1 mole% BaO_2.

Corroborating information was obtained from contact potential difference measurements. Relative changes in Ψ_0 compared to a standard silver catalyst for the series AgO/BaO_2 are shown in Fig. 7 (*22*). The data, representing a better average over the sample surface than with the small spots covered by the photoelectric method, were recorded at 25°C and 10^{-5} Torr. With increasing amounts of BaO_2 the contact potential becomes more positive with respect to an inert gold reference electrode. This corresponds to a decrease in work function. The results are in good agreement with the photoelectric data both qualitatively and quantitatively.

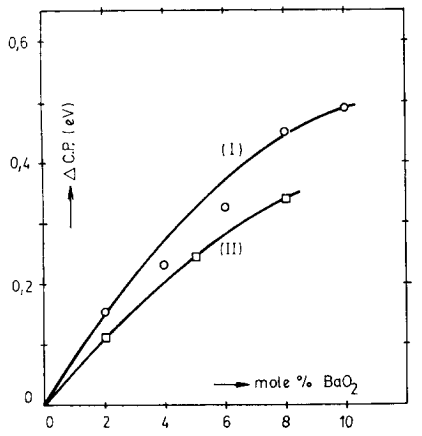

FIG. 7. Changes in contact potential ΔCP for Ag/BaO_2 catalysts (type I and II) at 25°C.

DISCUSSION

The most striking feature of the results is the marked decrease in work function of compound silver catalysts, most pronounced with small additive concentrations, and the fact that the emission characteristics are largely similar to those of a pure metal. This fact indicates that the photoelectrons originate directly in the metal phase, the potential barrier to be surmounted, however, having been reduced by some mechanism. Generally, the work function of a metal can be reduced without altering the photoemission characteristics by depositing on its surface a thin layer (typically a few monolayers thick) of a metal with low work function [e.g., Cs on Cu (*23*)]. Reduction in work function is also to be expected if the metal is covered with a thin film of a semiconductor, the work function of which should be lower than that of the metal. A thin layer of an insulator, however, would prevent any photoemission. Pure $BaCO_3$ and $SrCO_3$ being insulators (conductivity around 10^{-11} Ω^{-1} cm^{-1}), the lowered work function of compound silver catalysts can only be interpreted by assuming a thin carbonate coating covering the metallic silver which by incorporation of silver atoms as interstitials (donor levels) acquires semiconductor properties. It is very unlikely that metallic Ba or Sr are incorporated into the silver matrix and that due to their "electropositive" character relative to silver they are responsible for the reduced work function [this view, however, seems to have been tacitly assumed in some work dealing with changes in contact potential of silver catalysts modified by small amounts of "electropositive" elements (*3*, *4*)].

The model of a metal covered with a thin semiconducting carbonate film adopted in this study has been supported from scanning electron micrographs (*1*). The low electrical conductivity of the compound catalyst surfaces (as expected for a semiconducting film) could be directly observed from scanning electron micrographs by first exposing the surface to the electron beam at a magnification of 50× for a longer period and afterwards taking a photograph at a magnification of 20× (Fig. 8). The central field, intensively exposed to the electron beam, due to its *low electrical conductivity* is charged negatively relative to its surroundings (as seen from its darker appearance). This was not observed with pure silver catalysts or after coating the sample surface with gold as is usually done in scanning microscopy for poorly conducting samples.

Reduction in the work function of a metal by a semiconducting film is only feasible if the semiconductor has a work function lower than the metal, i.e., $\Psi_{SC} < \Psi_{Me}$. Thus, the carbonate film assumed here must have *n*-type characteristics because $\Psi_{BaCO_3} > \Psi_{Ag}$ and the necessary condition $\Psi_{BaCO_3/Ag} < \Psi_{Ag}$ can only be fulfilled if the carbonate is *n*-type due to incorporation of Ag atoms acting as donor levels.

The carbonate coating is formed during the conditioning period from additives that are not stable under reaction conditions. Due to the high mobility of the ions during this period (*1*) the coating is easily established as well as incorporation of silver atoms into the carbonate matrix, the ionic radii of Ag^+, Sr^{2+} and Ba^{2+} being 1.25 Å (atomic radius 1.44 Å), 1.13 Å and 1.35 Å, respectively. For type I catalysts the conditions for incorporating silver into the carbonate matrix are more favorable than for type II catalysts, the former having higher donor density. On the other hand, formation of the coating is facilitated with finely divided

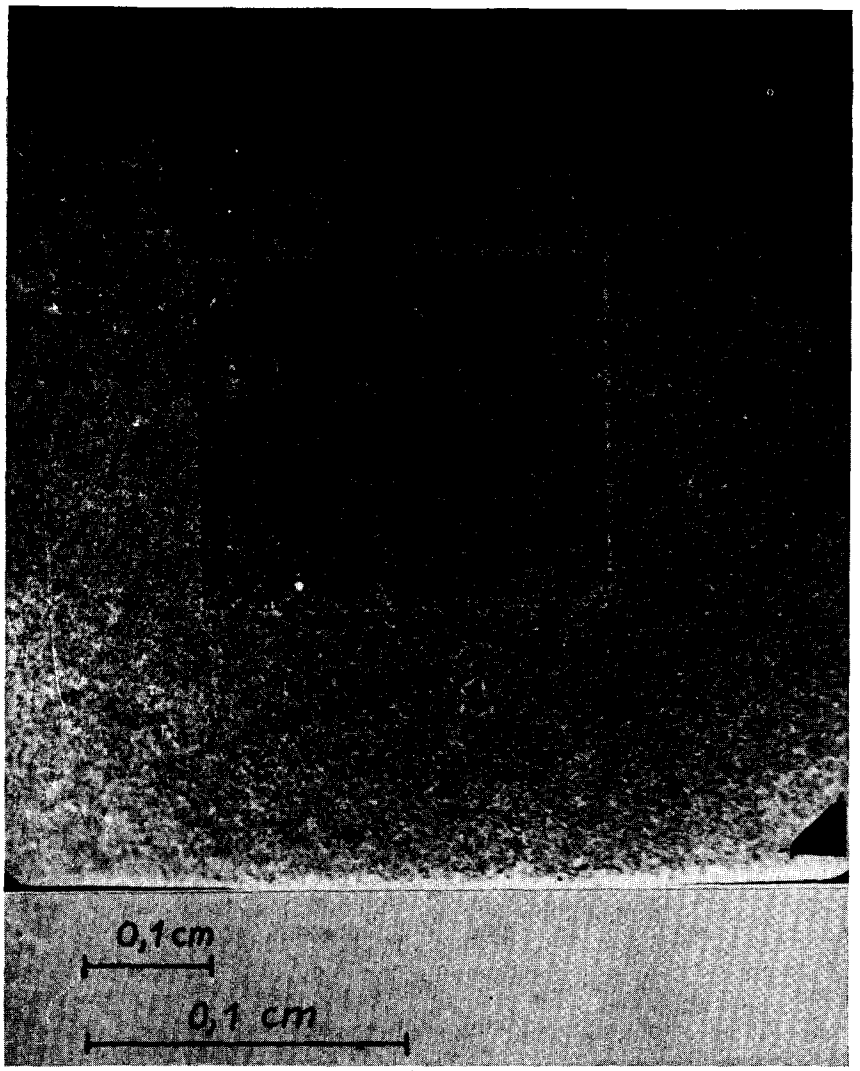

FIG. 8. Scanning electron micrograph of a Ag + 8 mole% BaO_2 catalyst revealing the poor electrical conductivity of the surface. Magnification 50× and 20×, respectively.

high surface area additives (peroxides) compared to well crystallized though powdered materials (formates). These features qualitatively explain the experimental findings summarized in Tables 2 and 3 and Figs. 5 and 6.

In the case of type I preparation, direct addition of the inert $BaCO_3$ also results in a reduced work function. Incorporation of silver into the carbonate is supported by vibration in alcohol where some AgO is reduced to metallic silver which at this time may be deposited in the pores of the carbonate giving rise to local low work function centers.

An attempt was made to simulate the postulated semiconducting carbonate by coprecipitation of Ag_2CO_3 and $BaCO_3$ followed by the usual conditioning procedure. The resulting compound did indeed have a specific conductivity of the order of magnitude for a semiconductor ($\sigma \simeq 10^{-2}\,\Omega^{-1}\,cm^{-1}$) and a work function of 3.8 eV, in line with the assumptions discussed above.

In any case, for compound silver catalysts of the type discussed in this article, the

catalytically active component cannot be considered to be a coherent matrix of metallic silver but rather a thin semiconducting carbonate layer in intimate contact with the metal. The actual *catalytic active sites at the carbonate surface* are imagined to be Ag^+ *ions* or *groups of* Ag^+ *ions* (ionized donors) which by *acquiring electrons* from the bulk (energetically from the Fermi potential at the outer surface) are developing chemical bonds with the acceptor gases (e.g., $Ag–O^{-\delta}$, $Ag–O_2^{-\delta}$, etc.). The density of these active sites might well be in the order of 10^{16} m^{-2}. The lower the work function at the semiconductor surface the less energy will be required to provide electrons at Ag^+ centers (ionized donors) and to form chemisorption complexes with the acceptor gases. The negative polarization of these complexes increases with decreasing work function. It is essential within this model that *silver atoms* are involved in the formation of the negatively charged chemisorption complexes, silver having been incorporated in the carbonate matrix during conditioning (see above). The important point is that the donor atoms (Ag) are assumed to be almost fully ionized and that they become catalytically active only after having received an electron from the bulk reservoir. The Fermi potential at the surface is essentially governed by the metal component and the donor density (Ag) in the semiconductor film and at its surface, respectively. Therefore it is justified to say that the "typical" properties of silver with respect to their catalytic oxidation behavior are still perceptible though modified by the semiconductor coating. Variations in electronic and catalytic properties with increasing amounts of an additive should arise from variation in the film thickness, the donor density and the specific surface area.

Assumption of a carbonate film covering the underlying metallic silver also accounts for the *common properties* of compound catalysts irrespective of the cation contained in the additive (Table 3).

According to Volkenstein (*24*) and others, most metals under reaction conditions are covered with a thin semiconducting film that governs the position of the Fermi level at the reaction interface and thus the actual catalytic characteristics. The thickness of the film should be small compared to the Debye length L_D in order that the metal properties still permeate it.

In the Volkenstein model the semiconducting component is thought of as a nonstoichiometric binary compound arising from the metal and one of the reacting species. For compound catalysts, such as those in this study, an extension of this model is proposed in that the semiconducting component is formed from suitable additives and, in contrast to binary films involving a gas component, the properties of the resulting catalysts are largely independent of reaction conditions, thus providing very stable catalysts. This has been proved experimentally (*1*, *2*).

In order to obtain an idea of the theoretical predictions of the position of the Fermi level at the reaction interface and the work function changes with varying thickness of the film compared to the experimental results, the electrostatic potential across the thin n-type semiconducting carbonate film in contact with metallic silver and the potential at the outer semiconductor/gas interface has been calculated. The methods of calculation are briefly outlined in the Appendix. For simplicity, it is assumed that the semiconducting carbonate film uniformly covers the silver matrix. The thickness of the film increases with increasing amounts of an additive and, e.g., at 10.5 mole% BaO_2 with a silver surface area of 0.8 m^2/g should be around 600 Å, a suitable value compared to a typical Debye length.

For the numerical calculations reasonable assumptions have been made for the donor density in the carbonate ($n_0 \simeq 10^{16}$ cm^{-3}) and for the adsorption equilibrium constant K of a possible acceptor reaction at the outer interface, i.e.,

$$\tfrac{1}{2}O_2 + e \rightleftarrows O_{ad}^-,$$

where $K = [O_{ad}^-]/\{n_0^- \cdot \exp(\bar{\phi}_{\tilde{L}}) \cdot p_{O_2}^{1/2}\} \simeq 0.5$ (Eq. A2). As pointed out above, the donor atoms (Ag) are assumed to be almost fully ionized. The potential at the metal–semiconductor interface was taken to be of the order of the maximum decrease in work

function with BaO_2 addition, i.e., $\Delta\Psi \simeq \phi_0 \simeq -0.6$ eV and $\bar{\phi}_0 \simeq -10$ in dimensionless units (at 300°C). The dimensionless parameter D_L given by Eq. (A13) thus becomes (with p_{O_2} in Torr units):

$$D_L \simeq 10^5 \cdot p_{O_2}^{1/2}$$

The results of the calculation are summarized in Fig. 9 as dimensionless potential $\bar{\phi}$ vs dimensionless coordinate $\bar{x}$. The lowest curve corresponds to the potential across an infinitely thick semiconductor film in the space charge region. The three upper curves apply to the potential $\bar{\phi}(\bar{L}) = \bar{\phi}_{\bar{L}}$ at the semiconductor/gas interface $\bar{L}$ for thin films and varying pressures of an acceptor gas (p_{O_2} = 0, 10^{-6} and 10^{-5} Torr, respectively). The broken lines show the potential *across* the film, $\bar{\phi}(\bar{x})$ for various values of $\bar{L}$ and p_{O_2}. The position of the *minimum*, at $\bar{x}_{1,i}$, of these functions corresponds to $\bar{\phi}_{\bar{L}}$ at zero pressure. Arrows indicate the decrease in work function (in dimensionless units) compared to silver for different situations.

On the basis of the data summarized in Fig. 9, changes in work function with increasing thickness of the carbonate film (increasing additive concentration) as well as the photoemission characteristics can be interpreted well. As found experimentally, Ψ_0 rapidly decreases with small additive concentrations and approaches a stationary value around 6–8 mole% addition. The calculated function $\bar{\phi}(\bar{L})$ semiquantitatively coincides with the measured Ψ_0 vs % additive relationship. The semiconducting film being very thin, the photoelectrons originate in the metal thus accounting for the observed emission characteristics typical for a metal. Absorption spectra taken from metallic silver and compound silver catalysts in the wavelength range of interest were qualitatively identical although absorption is more pronounced with compound catalysts. In a first step, interaction with photons raises the metal electrons to quantum states within the conduction band of the semiconducting film and from there, perhaps following interaction with thermal phonons, they are emitted from the semicon-

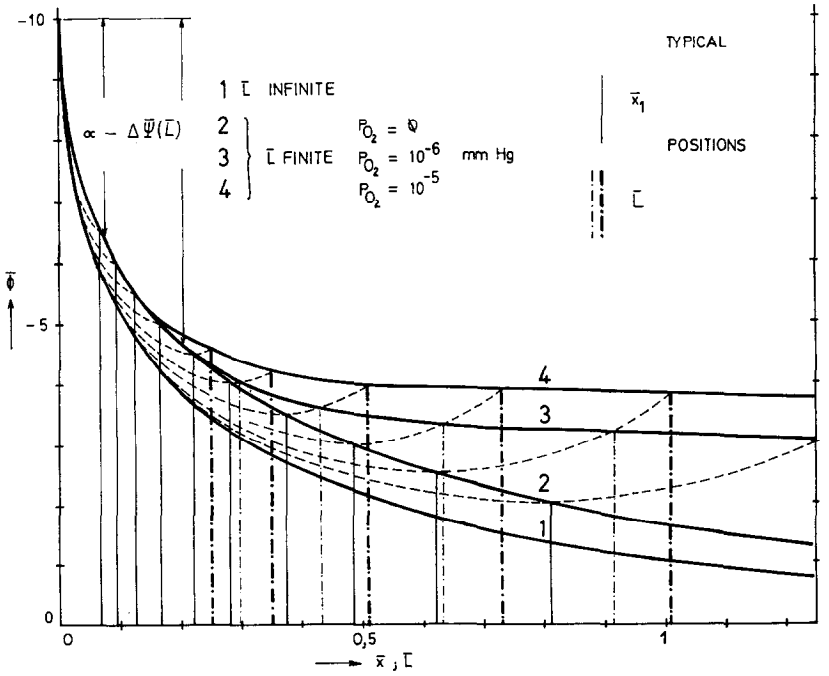

FIG. 9. Potential $\bar{\phi}$ across the semiconducting carbonate film at varying thickness $\bar{L}$ of the film in presence of 0, 10^{-6} and 10^{-5} Torr of an acceptor gas.

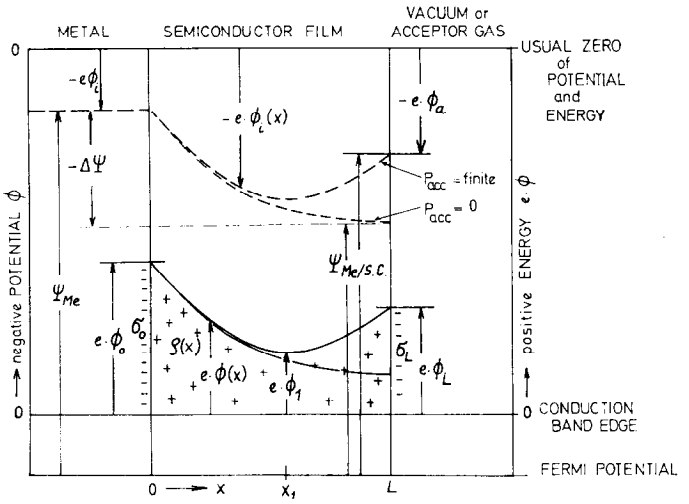

FIG. 10. Qualitative characteristics of the potentials involved within the system metal/semiconductor film/acceptor gas phase (p_{acc} = finite) and the system metal/semiconductor film/vacuum (p_{acc} = 0).

ductor surface. As seen from Figs. 9 and 10 the necessary photon energy will be lowered considerably with increasing film thickness. Figures 9 and 10 also explain the low emission current on adsorption of oxygen: with increasing p_{O_2} the energy bands at the semiconductor/gas interface are bent upwards, $\bar{\phi}_{\bar{L}}$ increases and the probability of electron emission at a given photon energy decreases. For ideal vacuum conditions the slope $(d\bar{\phi}/d\bar{x})_{\bar{x}=\bar{L}} = 0$ and there is no restraint for emission of photoelectrons.

The dependence of Ψ_0 on the cathode temperature may be due to different reasons which can operate in opposite directions:

1. Changes in catalyst configuration with increasing temperature. These changes occur very slowly and probably are only partially reversible. Ψ_0 is structure sensitive.
2. The Fermi potential at the semiconductor surface depends on both the temperature and the donor density.
3. Changes in residual oxygen chemisorption and degree of polarization at the semiconductor/gas interface with changes in temperature.

The temperature dependence of Ψ_0 being more pronounced with small additive concentrations is due to the fact that $(d/\bar{\phi}d\bar{L})_{\bar{L}}$ is considerably smaller with small $\bar{L}$ compared to larger ones.

The activity and selectivity of compound catalysts are strongly influenced by the electronic properties of the semiconductor/gas interface. Although the catalytic properties of Ag atoms (ionized donors + electrons from the bulk) persist, they are markedly modified by the semiconducting film of increasing thickness whereby electron transfer to the chemisorption complexes is facilitated. On decreasing the work function, activity strongly increases and selectivity decreases [cf. Fig. 9 in Ref. (*1*)]. The model stressed here implies that in addition to the strong increase in surface area with increasing additive concentration, changes of the electronic properties (Fermi potential) of the active interface must also be responsible for the marked changes in activity and selectivity. This also becomes obvious from the fact that the increase in activity with increasing additive concentration parallels the work function vs % additive characteristics. Both activity and Ψ_0 are most drastically altered at low additive concentration and at the same catalyst composition pass through a slight maximum [cf. Fig. 9 in Ref. (*1*)].

With reference to previous work (*1*, *2*) silver catalysts modified by addition of de-

composable alkaline earth compounds can be characterized as follows:

1. Catalysts of type I and type II preparation qualitatively behave the same, irrespective of the cation contained in the additive.

2. Type I catalysts have higher activity (lower work function) and lower selectivity as compared to type II catalysts of the same composition since the conditions for a properly developed carbonate coating are more favorable during homogenization of the components in alcohol.

3. At 6–8 mole% addition there is optimum doping of the carbonate film and the necessary condition $L < L_D$ is basically fulfilled. At higher additive concentration an optimum density of donor levels is no longer obtained, the worse for type II preparation, and the prerequisite for a proper metal/semiconducting film contact are no longer fully established.

4. The intrinsic reasons for activity and selectivity changes are certainly tied to altered chemisorption characteristics at the semiconductor/gas interface due to variations in the Fermi potential at the surface. Ionized donors (Ag^+) at the outer surface become catalytically active on receiving electrons from the bulk to build up chemisorption complexes with acceptor gases. Electron transfer from the bulk is governed by the position of the Fermi level at the surface. Decrease in work function with increasing L enhances the chemisorption capacity and polarization of an acceptor gas, e.g., oxygen, thus altering the relative rates of the rate determining steps with respect to formation of ethylene oxide or full oxidation of ethylene to $CO_2 + H_2O$. It is assumed that a less strongly polarized molecular oxygen species ($Ag–O_{2,ad}^-$) predominates at high work function surfaces, whereas a strongly polarized atomic species is favored at low work function surfaces. This would explain well the observed activity/selectivity characteristics if one agrees that the species $O_{2,ad}^-$ is responsible for formation of ethylene oxide and the atomic oxygen species O_{ad}^- brings about full oxidation of ethylene to $CO_2 + H_2O$ (*25*). The charges at the chemisorbed species are not necessarily integral.

Appendix

In this Appendix a method for numerically solving Poisson's equation valid within the semiconducting region of the system, metal/semiconductor film/gas phase, is briefly outlined which is based upon a concept qualitatively developed by Volkenstein (*24*). The purpose of these calculations is to obtain a theoretical view of the potential across the semiconducting film as well as at its outer surface on varying the film thickness and the partial pressure of an acceptor gas at the gas/solid interface. Variation of the Fermi potential and the work function at this interface will strongly influence the chemisorption characteristics and thus the catalytic properties. Since only the salient features of the model need be emphasized the calculations are carried out with largely idealized assumptions (uniform film, homogeneous doping, etc.).

A metal/n-type semiconducting film contact with $\Psi_{Me} > \Psi_{SC}$ is characterized by a positive space charge $\rho(x)$ within the semiconductor region ($L \geq x \geq 0$) balanced by the negative charge σ_0 at the metal/semiconductor interface and in the case of chemisorbed acceptor species also by the negative charge σ_L at the outer surface L. The potential characteristics across the thin semiconductor film confined to a metal and an acceptor gas interface (or a vacuum) are qualitatively shown in Fig. 10. ϕ_0 is the (negative) potential at the metal/semiconductor interface (diffusion potential) due to electron flow from the film into the metal. ϕ_i and ϕ_a are the inner and outer electrostatic potential, respectively. The thickness of the film should be smaller than the Debye length, i.e., $L < L_D$. It is only then that the properties of the metal permeate the film. Increase in ϕ_i will be accompanied by a corresponding decrease in work function Ψ. For convenience, however, instead of calculating ϕ_i or ϕ_a we shall deal with the quantity $\phi(x)$ which is proportional to the work function Ψ. Thus, the zero of the potential is put equal to the conduction band edge far away from the metal/semiconductor interface. The potentials and energies are counted negatively and positively upwards, respectively.

In presence of an acceptor gas (with

electronegativity exceeding that of the metal) chemisorbed at the outer surface according to the idealized equation

$$\tfrac{1}{2}O_2 + e \rightleftarrows O_{ad}^- \qquad (A1)$$

(e is an electron in the conduction band of the film) the function $\phi(x)$ is bent upwards at the outer surface, the minimum position being at x_1. The equilibrium constant applying to Eq. (A1) is defined by

$$K = \frac{[O_{ad}^-]}{n^-(L) \cdot p_{O_2}^{1/2}}, \qquad (A2)$$

where $n^-(L)$ and $[O_{ad}^-]$ denote the electron concentration at point L and the concentration of chemisorbed O^- atoms.

The electrostatic potential $\Psi(x)$ within the film is governed by Poisson's equation,

$$d^2\phi/dx^2 = -4\pi\rho\{\phi(x)\}/\epsilon, \qquad (A3)$$

where ϵ is the dielectric constant of the film with boundary conditions:

$$(d\phi/dx)_{x=L} = 4\pi\sigma_L/\epsilon \qquad (\sigma_L < 0), \qquad (A4)$$

$$\phi(x = 0) = \phi_0. \qquad (A5)$$

If n_0^- and n_0^+ denote the concentration of free negative and positive charge carriers at the point where $\phi = 0$ then the concentrations $n^-(x)$ and $n^+(x)$ at any position x will be given by

$$n^+ = n_0^+ \cdot \exp\{-e\phi(x)/kT\}, \qquad (A6)$$

$$n^- = n_0^- \cdot \exp\{+e\phi(x)/kT\}, \qquad (A7)$$

whence

$$n_0^+ = n_0^- = n_0, \qquad (A8)$$

to ensure electroneutrality. The space charge function $\rho\{\phi(x)\}$ within the film thus may be written

$$\rho\{\phi(x)\} = e \cdot \{n^+(x) - n^-(x)\} = 2e \cdot \sinh\{e\phi(x)/kT\}. \qquad (A9)$$

The charge σ_L at the film/gas interface according to Eq. (A2) is obtained from

$$\sigma_L = -e \cdot [O_{ad}^-] = -e \cdot n_0 \cdot K \cdot p_{O_2}^{1/2} \cdot \exp\{e\phi_L/kT\}. \qquad (A10)$$

Introducing dimensionless variables (marked by a bar)

$$\bar{\phi} = e\phi/kT \qquad \bar{x} = \{(4\pi e^2 \cdot n_0)/(\epsilon kT)\}^{1/2} \cdot x \qquad (A11)$$

Eqs. (A3) to (A5) become:

$$d^2\bar{\phi}/d\bar{x}^2 = 2 \cdot \sinh(\bar{\phi}), \qquad (A12)$$

$$(d\bar{\phi}/d\bar{x})_{\bar{L}} = -\{(4\pi e^2 \cdot n_0 \cdot K \cdot p_{O_2}^{1/2})/(\epsilon kT)\}^{1/2} \cdot \exp\bar{\phi}_{\bar{L}} = -D_L \cdot \exp\bar{\phi}_{\bar{L}} = \bar{\sigma}_{\bar{L}}, \qquad (A13)$$

$$\bar{\phi}(\bar{x} = 0) = \bar{\phi}_0. \qquad (A14)$$

Integration of Eq. (A12) within the regions $0 \leq \bar{x} \leq \bar{x}_1$ and $\bar{x}_1 \leq \bar{x} \leq \bar{L}$ yields

$$\left(\frac{d\bar{\phi}}{d\bar{x}}\right)^2_{\bar{x},\bar{x}_1} - \left(\frac{d\bar{\phi}}{d\bar{x}}\right)^2_0 = 4\{\cosh\bar{\phi}(\bar{x}), \bar{\phi}_1 - \cosh\bar{\phi}_0\}, \qquad (A15)$$

$$\left(\frac{d\bar{\phi}}{d\bar{x}}\right)^2_{\bar{x},\bar{x}_1} - \left(\frac{d\bar{\phi}}{d\bar{x}}\right)^2_{\bar{L}} = 4\{\cosh\bar{\phi}(\bar{x}), \bar{\phi}_1 - \cosh\bar{\phi}_{\bar{L}}\}. \qquad (A16)$$

Since $(d\bar{\phi}/d\bar{x})_{\bar{x}_1} = 0$ the charge $\bar{\sigma}_{\bar{L}}$ at the surface $\bar{x} = \bar{L}$ is given by

$$\bar{\sigma}_{\bar{L}} = -(d\bar{\phi}/d\bar{x})_{\bar{L}} = -D_L \cdot \exp/\{\bar{\phi}_{\bar{L}}\} = 2(\cosh\bar{\phi}_{\bar{L}} - \cosh\bar{\phi}_1)^{1/2}. \qquad (A17)$$

For idea vacuum conditions (i.e., $D = 0$) $\bar{\phi}_{\bar{L}} = \bar{\sigma}_1$ and $\bar{\sigma}_{\bar{L}} = 0$.

Given $\bar{\phi}_0$ from the known characteristics of the metal/semiconductor interface as well as D_L from Eq. (A13) and using reasonable assumptions for n_0 and K, $\bar{\phi}_{\bar{L}}$ can be calculated from Eq. (A17) for any chosen $\bar{\phi}_1$. The function $\bar{x}(\bar{\phi})$ within the regions $0 \leq \bar{x} \leq \bar{x}_1$ and $\bar{x}_1 \leq \bar{x} \leq \bar{L}$ are found by numerical integration of

$$\bar{x}(\bar{\phi}) = \int_{\bar{\phi}_0}^{\bar{\phi} \leq \bar{\phi}_1} \frac{d\bar{\phi}}{2 \cdot (\cosh\bar{\phi} - \cosh\bar{\phi}_1)^{1/2}} \qquad 0 \leq \bar{x} \leq \bar{x}_1, \qquad (A18)$$

$$(\bar{L} - \bar{x})(\bar{\phi}) = \int_{\bar{\phi}_{\bar{L}}}^{\bar{\phi} \geq \bar{\phi}_1} \frac{d\bar{\phi}}{2 \cdot (\cosh\bar{\phi} - \cosh\bar{\phi}_1)^{1/2}} \qquad \bar{x}_1 \leq \bar{x} \leq \bar{L}. \qquad (A19)$$

References

1. Spath, H. T., Tomazic, G. S., Wurm, H., and Torkar, K., *J. Catal.* **26**, 18 (1972).
2. Spath, H., and Torkar, K., *J. Catal.* **26**, 163 (1972).
3. Margolis, L. Ya., Enikeev, E. Kh., Isaev, O. V., Krylova, A. V., and Kushnerov, M. Y., *Kinet. Katal.* **3**, 181 (1962).
4. Margolis, L. Y., *in* "Advances in Catalysis" (D. D. Eley, H. Pines and P. B. Weisz, Eds.), Vol. 14, p. 429. Academic Press, New York, 1963.

5. VOGE, H. H., AND ADAMS, C. R., *in* "Advances in Catalysis" (D. D. Eley, H. Pines and P. B. Weisz, Eds.), Vol. 17, p. 151. Academic Press, New York, 1967.
6. WOLF, F., AND GÖTZE, H., *Chem. Tech. (Berlin)* **14,** 600 (1962).
7. WAN, S.-W., *Ind. Eng. Chem.* **45,** 243 (1953).
8. MURRAY, K. E., *Aust. J. Sci. Res., Ser. A* **3,** 443 (1950).
9. MCBEE, E. T., HAAS, H. B., AND WISEMAN, P. A., *Ind. Eng. Chem.* **37,** 432 (1945).
10. FOGNANI, F., AND MONTARNAL, R., *Rev. Inst. Fr. Petrole Ann. Combust. Liquides* **14,** 191 (1959).
11. BRENGLE, A. S., EL SOBRANTE, AND STEWART, H. R., *US Pat.* 2,709,173 (1955).
12. KEITH, C. D., HINDIN, S. G., AND GALEN, L. A., *US Pat.* 3,423,328 (1969).
13. SANDLER, Y. L., AND DURIGON, D. D., *J. Phys. Chem.* **69,** 4201 (1965).
14. KUMMER, J. T., *J. Phys. Chem.* **60,** 666 (1956).
15. FOWLER, R. H., *Phys. Rev.* **38,** 45 (1931).
16. "Handbook of Chemistry and Physics," 48th ed., E 71 (1967/68).
17. WINCH, R. P., *Phys. Rev.* **37,** 1269 (1931).
18. SUHRMANN, R., AND WEDLER, G., *Z. Angew. Phys.* **14,** 70 (1962).
19. D'ANS-LAX, Taschenbuch für Chemiker und Physiker, Vol. 3, p. 258. Springer Verlag, Berlin, 1970.
20. MILLIKAN, R. A., *Phys. Rev.* **30,** 287 (1910).
21. WINCH, R. P., *Phys. Rev.* **38,** 321 (1931).
22. SPATH, H. T., PRIESCHING, D., AND TORKAR, K., unpublished data.
23. BERGLUND, C. N., AND SPICER, W. E., *Phys. Rev.* **136,** 1044 (1964).
24. VOLKENSTEIN, T., "Elektronentheorie der Katalyse an Halbleitern," VEB Deutscher Verlag der Wiss., Berlin, 1964.
25. SPATH, H. T., *Proc. Int. Congr. Catal., 5th,* (Palm Beach, FL) *1972,* 945 (1973).